

Properties of Thermally Dewetted Thin Au Films on ITO-Coated Glass for Biosensing Applications

Katarzyna Grochowska¹  · Katarzyna Siuzdak¹ · Jakub Karczewski² · Mariusz Szkoda^{1,3} · Gerard Śliwiński¹

Received: 23 August 2016 / Accepted: 25 November 2016 / Published online: 8 December 2016
© Springer Science+Business Media New York 2016

Abstract Noble metal nanostructures are object of great interest due to their unique optical and electronic properties exploited in nanotechnology, medicine, biochemistry, and surface-enhanced spectroscopies. In this work, the Au nanoparticle (NP) structures for application in biosensing obtained by dewetting are investigated in dependence on their preparation conditions. Structures are produced from thin Au films (5–30 nm) sputtered onto the ITO-coated glass substrates. The dewetting is performed by thermal treatment in ambient air. SEM inspection of the structures reveal breakup of the Au films into NPs of rounded shape. The NP size does not exceed 80 nm and their shape can be tuned by duration of the dewetting. In the absorbance spectra, the broad peaks centered around 550–620 nm are ascribed to resonant absorption of the surface plasmons and the estimated time of resonance damping is in the range of 2.24–3.65 fs. The large signal values observed in Raman spectra, and the electrochemical performance confirm that the produced material can serve as an electrode for sensing applications.

Keywords Au nanoparticles · AuNPs/ITO electrodes · SERS measurements · Electrochemical methods

✉ Katarzyna Grochowska
kgrochowska@imp.gda.pl

¹ Centre for Plasma and Laser Engineering, Szewalski Institute of Fluid-Flow Machinery, Polish Academy of Sciences, Fiszerza 14 St., 80-231 Gdańsk, Poland

² Faculty of Applied Physics and Mathematics, Gdańsk University of Technology, Narutowicza 11/12 St., 80-233 Gdańsk, Poland

³ Faculty of Chemistry, Gdańsk University of Technology, Narutowicza 11/12 St., 80-233 Gdańsk, Poland

Introduction

The production and characterization of noble metal nanoparticle (NP) arrays have been the subject of intense studies due to their specific optical properties such as the surface plasmon resonance (SPR) absorption. It is well known that interaction of free electrons in the metal with light induces their resonant oscillations and hence the enhancement of the electric field on the metal NP surface. However, the resonance condition strictly depends on the size, shape, and dielectric constants of the metal and the surrounding material [1, 2]. Even the small change in shape and size of the NPs causes modification of the profile of plasmon resonant absorption, whereas changing the dielectric constant of the surrounding material results in a shift of the absorption maximum. These unique properties of noble metal NPs allow their usage in such areas as photonics [3], catalysis, and electrocatalysis [4, 5] or in the sensing and imaging techniques [6, 7]. Though, all those applications require the fabrication of NP arrays of controlled size, spacing, and ordered distribution, which is very challenging especially in terms of obtaining desired structures on large areas. In general, there are two routes to produce metal NPs: the bottom-up, where atoms and molecules are assembled to generate nanostructures, or top-down, where structures are formed after removing of material from bulk. Common bottom-up techniques are wet chemical synthesis/deposition including dip-coating, spin-coating, and Langmuir-Blodgett methods [8]. Although those techniques allow producing thin metallic layers, it is nearly impossible to obtain NP arrays characterized by monodispersity and long-range periodicity. The top-down techniques, such as the photo [9], electron beam [10, 11], focused ion beam [12], and scanning probe [13] lithographies, allow forming well-defined and well-ordered NP arrays. On the other hand, the commercially available instrumentation is expensive which highly influence the usage of

these methods at industrial scale. This problem can be omitted by using thermal dewetting/annealing or pulsed laser-induced thermal dewetting conducted under vacuum conditions (PLiD) [14–18]. Compared to other techniques, the thermal annealing is relatively non-time consuming and less cost effective. Moreover, we have recently demonstrated that PLiD can be used to create NP arrays of the areas of $4 \times 4 \text{ mm}^2$ which can be multiplied by the spot by spot repetition that allows producing structures of defined, larger areas dedicated to specific applications [19]. Although, applications of the PLiD technique are limited by dimensions of the vacuum chamber systems and dewetting in the air is not acceptable because it can lead to contamination of the prepared samples. That is why in order to obtain the desired, large area structures in the one-step procedure, we propose in this work the thermal dewetting in the furnace to produce arrays of areas of $10 \times 10 \text{ mm}^2$. The glass coated by indium tin oxide (ITO) layer is used as substrate for deposition of the metal thin films. The selected material is characterized by low electrical resistivity and good optical transparency, high reflectivity and absorption in UV, visible, and infrared regions, respectively [20–22]. ITO coatings evoke continuous interest in previously reported biosensing applications [23–25]. However, for such applications, both the transparent (ITO or fluorine tin oxide (FTO) [26, 27]) or non-transparent (glassy carbon [28, 29]) materials can be exploited.

In this work, the thermal dewetting is applied to produce gold nanoarrays consisting of nearly spherical and disk-like NPs on ITO substrates. Gold is selected as a model metal because of its high chemical stability and biocompatibility. However, the Au NPs obtained in this process are more irregular in shape in comparison to those fabricated by pulsed laser irradiation [19, 26]. It is shown that by changing the time of the annealing, it is possible to obtain regularly distributed nanoparticles of the almost spherical form. The reported structures of the controlled NP geometry (shape, size) and interparticle distances cover a large surface area ($10 \times 10 \text{ mm}^2$). The positive effect of the structural properties of ITO modified with Au NPs observed via enhancement of the Raman signal and also enhanced electrochemical activity toward glucose is reported and discussed.

The obtained results indicate that the proposed fabrication method of the electrode material can meet all demands required for application at industrial scale. Therefore, it deserves further attention and development.

Experimental

Materials

KCl (99.5%), KOH (85%), and $\text{K}_3\text{Fe}(\text{CN})_6$ (99.8%) were purchased from POCH, while ethanol, acetone, isopropanol,

and glucose (optical rotation $+52.5$ – 53°) were obtained from Chempur. Rhodamine 6G and thin ITO films deposited on polished soda lime glass (thickness 100 nm, absorption at 550 nm ca. 16%) were purchased from Sirah and Ossila LTD, respectively. All chemicals were used without any further purification. The ITO-coated substrates were sonically cleaned in the abovementioned alcohols and in the deionized water. The metal target used for sputtering (Au, purity 99.99%) was obtained from Quorum Technologies.

Metal Sputtering

Au thin films were deposited onto a chemically cleaned ITO-coated soda lime glass using a RF Emitech K550X sputter coater. The sputtering was performed at room temperature and at pressure of 4×10^{-2} hPa in the presence of high-purity Ar. The thickness of the metal films was controlled in the range between 5 and 30 nm and the film growth rate was equal to 7.5 nm/min.

Electrode Preparation by Thermal Dewetting

The Au-coated samples were annealed in the muffle furnace (Neotherm) in the air under ambient pressure and temperature in the range of 400–700 °C. Samples were put into the furnace after the process temperature was reached. The dewetting time has been selected from the range of 5–90 min. After annealing, the samples were removed from the furnace and rapidly cooled down to room temperature.

Characterization of the Electrodes

Field emission scanning microscopy (SEM) (FEI Quanta FEG 250 with ET secondary electron detector and beam accelerating voltage kept at 10 kV) was applied to study the morphology of the prepared materials. The UV-Vis spectrophotometer (Perkin-Elmer Lambda 18) was used to obtain absorbance data. SERS and electrochemical measurements were performed by means of the micro-Raman microscope (inVia, Renishaw, excitation wavelength 514 nm, magnification $\times 50$) and the potentiostat-galvanostat system AutoLabPGStat 302 N in a standard three-electrode assembly at 295 K, respectively. Pt mesh served as a counter electrode (CE) and Ag/AgCl/0.1 M KCl was used as reference one (REF). Au layers before (Au-5 nm) and after thermal annealing (Au-5 nm-X min, where X denotes the dewetting duration) deposited onto the ITO substrates stayed as a working electrode (WE). For comparison, the Au gold disk electrode (mineral, 2 mm in diameter) and the clean ITO substrate were tested as well. The electrode material was put into the specimen holder made from polyether ether ketone material which enabled a strictly defined contact area between the electrode surface and electrolyte. The diameter of the circular sample

area wetted by electrolyte was 3 mm. Correspondingly, all current densities given in this work were calculated on the basis of the geometric surface area. Before the electrodes were used, they were rinsed with water and then dried under nitrogen stream. Cyclic voltammetry tests were performed in solutions: 10 mM $\text{K}_3\text{Fe}(\text{CN})_6$ + 1 M KCl and 0.1 M KOH with addition of 10 mM of glucose. All the electrolytes were purged with argon for 50 min before electrochemical tests, and during measurements, there was an Ar-cushion above the electrolyte.

Results and Discussion

For the thin Au films (5, 10, 20, and 30 nm) deposited onto ITO substrates and annealed in the furnace under the temperatures in the range of 400–700 °C for up to 90 min, the Raman spectra were preliminarily recorded in order to validate the sensing capability of the produced samples. After procedure optimization, the best results defined as the highest enhancement of the Raman signal for rhodamine 6G (model molecule) were obtained for samples prepared from 5-nm thick Au films annealed at 500 °C for 80 min. Samples dewetted at the same temperature but for shorter time (5 and 50 min) were also investigated to confirm the best results in terms of the highest peak current observed during electrochemical measurements. Moreover, pure ITO substrates were also processed under the same conditions as the Au-modified ones to provide the reference and to check the change in resistivity of the oxide layer. The increase of resistivity from ca. 25 Ω (unprocessed ITO) to ca. 150 Ω (ITO glass annealed for 90 min) was observed.

Morphology and Optical Properties of the Au NPs/ITO Electrodes

As it is shown in Fig. 1a, the sputtered 5-nm thick Au layer is free of any surface defects and cracks. Such uniformity is observed on the whole $10 \times 10 \text{ mm}^2$ area of the sample. Also, from the magnified view in Fig. 1b, it can be concluded that the obtained metallic films are granular and no discontinuities are

observed. This high-surface quality of the Au layer confirms the substrate material data too, as the roughness of the ITO coating and glass substrate are less than 1.8 and 1 nm, respectively.

The thermal dewetting of the thin Au films and the resulting formation of the nanoparticles originates in the known high interfacial tension of metals on oxide surfaces [30]. It should be mentioned that at temperatures around 900–1200 °C, various surface processes, e.g., metal-substrate chemical interactions and metal diffusion into the substrate, can influence the annealing [31]. However, this problem is omitted here as the temperature required to induce the melting of Au thin films is ca. 400–450 °C. On the other hand, for other metallic particles, the thermal dewetting process is therefore limited to thin metal layers showing low melting point [30].

The evolution of the metallic thin films during thermal treatment is shown schematically in Fig. 2. The layer fragmentation starts at the grain boundaries when the required temperature is reached. Further annealing results in formation of islands of irregular shapes and spacing. Prolonged processing at elevated temperature causes the splitting of islands into nanoparticles; therefore, the final geometry of the NP structure, that is, NP shape and structure regularity, depends strictly on the annealing time.

The surface inspection by means of SEM images of the prepared electrodes indicates that the obtained nanoparticles are disk-like (top inset of Fig. 3a) and nearly spherical (top insets of Fig. 3b, c) in shape in dependence on annealing time. Moreover, from the FFT patterns (see down insets), the regularity of the structures can be concluded and the mean interparticle distances of 56 ± 11 , 51 ± 10 , and 37 ± 7 nm for samples processed for 5, 50, and 80 min, respectively, are estimated. The coverage of ITO by Au NPs exceeds 15–25% for all prepared samples, and this value is slightly higher than reported for laser dewetted electrodes [17]. From the size distributions extracted from SEM images in Fig. 3, the average NP size of 35 ± 13 , 36 ± 10 , and 40 ± 11 nm are obtained—see Fig. 4.

The NP dimensions can be verified using data derived from the UV-Vis spectra as their profile lines and maximum peak

Fig. 1 a SEM image of the 5-nm Au layer deposited onto ITO-coated soda lime glass; b $\times 10$ magnification of the structure shown in a

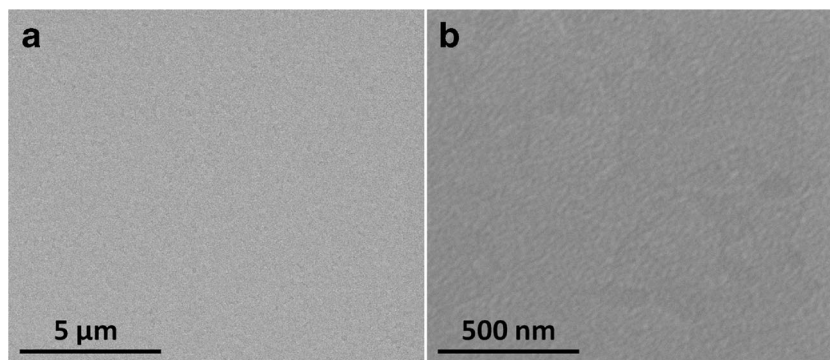
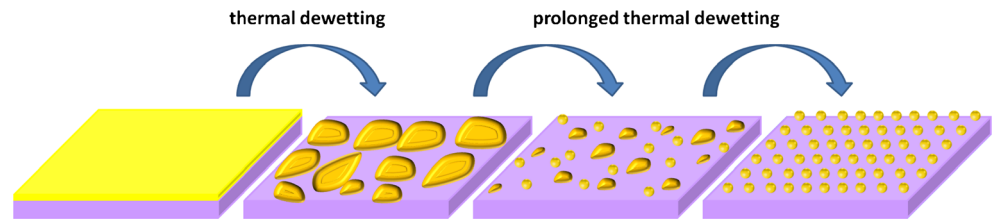


Fig. 2 Evolution of the dewetting of metal thin film deposited onto ITO substrate during thermal treatment: from unaffected film to formation of spherical particles



positions strictly depend on the shape and size of the particles. For spherical and nearly spherical NPs of diameter in the range of 35–110 nm, a semiempirical relation proposed by Haiss et al. [32] can be applied:

$$d[\text{nm}] = \frac{\ln\left(\frac{\lambda_{\text{SPR}} - \lambda_0}{L_1}\right)}{L_2} \quad (1)$$

where $\lambda_0 = 512$ nm, $L_1 = 6.53$, and $L_2 = 0.0216$. This relation is sufficiently precise (accuracy better than 3%) for refractive index of 1.33 of the surrounding medium. In our previous work [19], according to the approach proposed by Simsek [33], we proved that NPs supported on ITO-coated glass can be treated as NPs suspended in water (effective refractive index of such system is ca. 1.3–1.33). Nevertheless, in that case, the inaccuracy of relation (1) increases up to 10%. The absorbance spectra of the prepared electrodes are shown in Fig. 5, and from resonance positions, the size of 90 nm for NPs shown in Fig. 3b, c is estimated. This value is about twice as bigger as the values estimated from size distributions. Also, the resonance band is significantly more red shifted than expected when taking into account the average NP diameters obtained from the SEM images. However, the value of 90 nm corresponds to the size of largest particles formed during the dewetting process (see Fig. 4). Therefore, it can be assumed that the values extracted from the UV-Vis spectra and SEM images are in reasonable agreement.

From the performance point of view of a sensor based on the plasmonic effect, the damping of SPR is of key importance as the electrode performance rises with

longer dephasing time. The total dephasing of the plasmons is given by:

$$\frac{1}{T_2} = \frac{1}{2T_1} + \frac{1}{T_2^*} \quad (2)$$

where T_1 —inelastic population decay time constant and T_2^* describes the elastic dephasing processes. The knowledge of the dephasing mechanisms is essential for a large variety of applications (especially sensing) and is thoroughly discussed elsewhere [34, 35]. In the dephasing time estimation, the relation with measured resonance width (Γ , FWHM—see Fig. 5 inset) can be applied:

$$T_2 = \frac{2\hbar}{\Gamma} \quad (3)$$

Values of T_2 calculated for the 5-nm thick Au films dewetted at 500 °C are presented in Table 1. It can be easily seen that for shorter annealing durations, the dephasing time rises observably with prolonged sample exposure to the elevated temperature. This behavior is observed for annealing time up to 50 min. After that, the equilibrium is reached. Therefore, based on the estimations, the best results in terms of sensing should be obtained for samples annealed for at least 60 min. This is confirmed by Raman measurements.

Electrode Performance

Spectroscopic Properties

The quantitative data on the SERS signal provide a quick and reliable verification of the properties required in detection

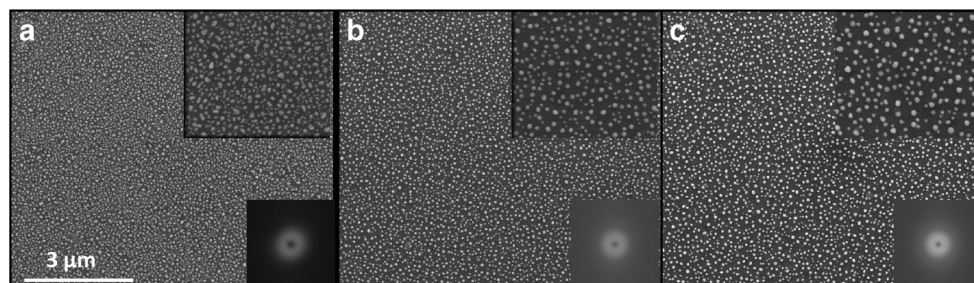


Fig. 3 Top view of the Au NP arrays obtained from Au films of a thickness of 5 nm thermally dewetted for 5 (a), 50 (b), and 80 min (c); top insets depict the evolution of NP shape: from disk-like (a) to nearly

spherical (b, c), and down insets show power distributions of FFT-processed SEM images

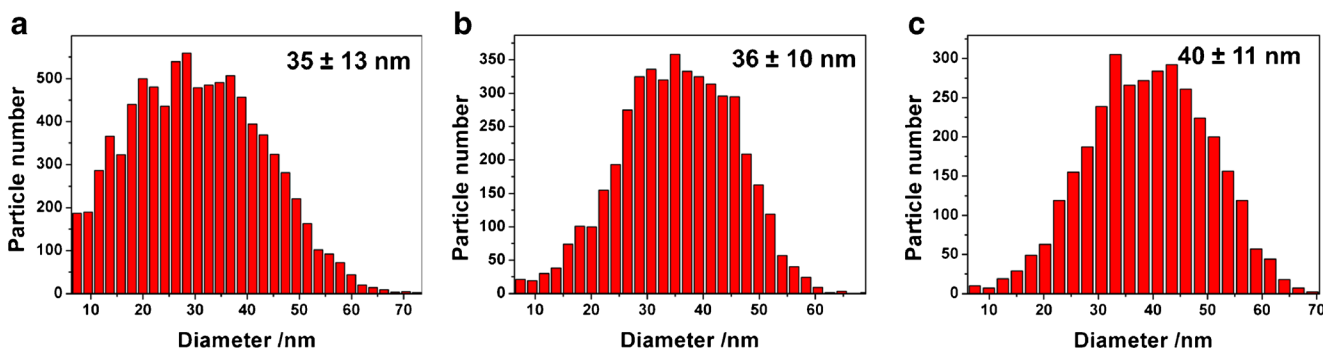


Fig. 4 Size distributions of NP arrays with the mean diameter values; diagrams in **a**, **b**, and **c** corresponding to images of Fig. 3a–c

based on plasmonic effect [36]. The Raman spectra of rhodamine 6G (R6G) diluted in ethanol (concentration 10^{-6} M) deposited and dried on different Au-modified ITO substrates are shown in Fig. 6. From comparison of spectra, the distinctly higher Raman peak intensities can be observed for NP structures produced via prolonged thermal dewetting, i.e., annealing time exceeds 50 min, while the spectra of NPs obtained via a short-time processing (5 min) and of untreated metal film show only weak signals of the characteristic peaks. This observation is in agreement with the granular morphology of thin unprocessed layers visible in the SEM images.

The enhancement factor (EF) of the Raman signal can be estimated from given relation [37]:

$$EF = \frac{I_{SERS}/N_{SERS}}{I_R/N_R} \quad (4)$$

where: I_{SERS} , I_R —intensities of SERS and Raman signals; N_{SERS} , N_R —number of molecules contributing to SERS and Raman intensities, respectively. However, in the case when values of N_{SERS} and N_R are unknown and there is no Raman

signal recorded for bulk samples, the approach thoroughly described in [38] can be applied in evaluation of EF. Briefly, the estimation of EF is based on the comparison between Raman and fluorescence intensities for the studied molecule. Under applied excitation at 514 nm, the intensity of the fluorescence signal at 1355 cm^{-1} is 1.2×10^4 , while the intensities of the corresponding Raman peaks in spectra of dewetted samples are in the range of $(0.5\text{--}1.4) \times 10^5$. The fluorescence cross-section of R6G and Raman scattering cross-section are known and equal to 10^{-16} cm^2 at 514 nm and 10^{-30} cm^2 , respectively [38]. Given that and assuming constant ratio of illuminated Au and R6G molecules of about 10^3 [39], and taking into account that Raman scattering of R6G is enhanced by about 10^4 due to resonance at 514 nm, the EF of $10^7\text{--}10^8$ for prepared samples can be estimated. Nevertheless, from the point of view of sensing capability, the NP arrays processed for 80 min are candidates showing the best performance as the observed Raman signal is almost two and four times larger than registered for samples processed for 50 and 5 min, respectively.

Electrochemical Activity

The cyclic voltammetry curves (CVs) recorded in ferricyanide solution for various electrode materials are shown in Fig. 7. The shape of CV allows evaluating response toward faradaic reaction depending on the electrode elements (i.e., the single NPs) and the time scale of the experiment [40]. From the current-potential dependence obtained at scan rate of 50 mV/s, the ITO and Au disk electrode are characterized by the lowest current density and the smallest difference between anodic and cathodic potential peaks (ΔE). In the case of Au-modified electrode, the current density at peaks corresponding to the oxidation and reduction process of $\text{Fe}^{2+}/\text{Fe}^{3+}$ are significantly higher but simultaneously ΔE increases. The increase in current corresponding to faradaic reaction demonstrates that ITO/Au materials possess a higher active surface area due to the presence of nanoparticles [41]. The relation of the peak current follows the order Au-5 nm-5 min < Au-5 nm-50 min < Au-5 nm-80 nm that corresponds to the relation of

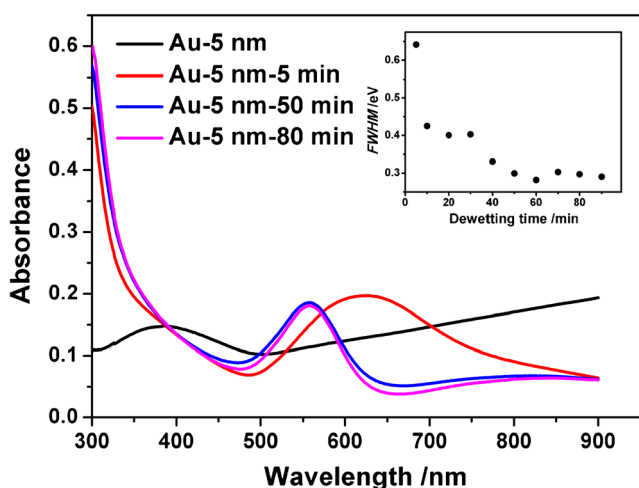


Fig. 5 Absorbance spectra of electrodes prepared from 5-nm thin gold films; *black*—unprocessed (no thermal treatment), *red*—annealing time (t_a) of 5 min, *dark blue*— $t_a = 50$ min, *orange*— $t_a = 80$ min. *Inset* shows the width of the resonance plotted as a function of dewetting time

Table 1 Bandwidth of the resonance profile and dephasing time values estimated for structures prepared from 5-nm thin Au films annealed at 500 °C

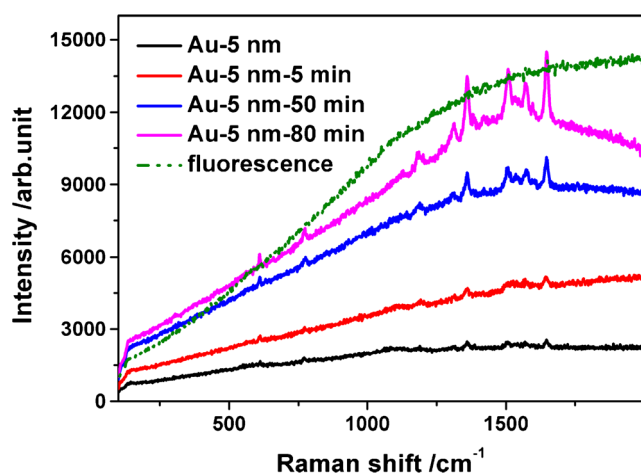
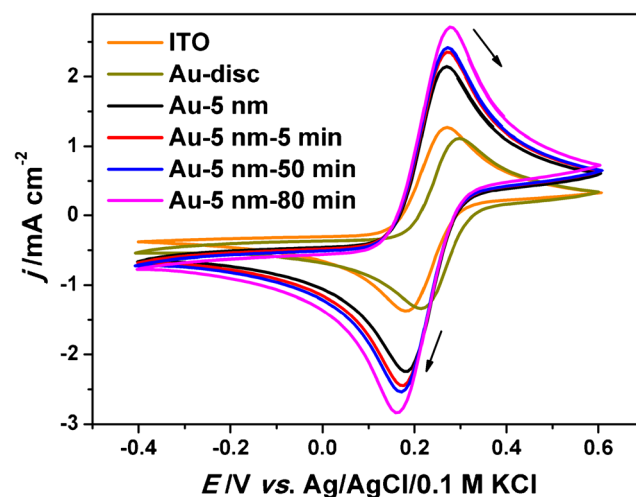
t (min)	5	10	20	30	40	50	60	70	80	90
$FWHM$ (eV)	0.59	0.47	0.43	0.42	0.38	0.37	0.37	0.36	0.37	0.37
T_2 (fs)	2.24	2.78	3.05	3.11	3.47	3.59	3.59	3.65	3.57	3.58

interparticle distances and the mean NP diameter (see the “Morphology and optical properties of the Au NPs/ITO electrodes” section). For the Au/ITO thermally treated for 5, 50, and 80 min, the difference between reduction and oxidation potential equals 0.096, 0.102, and 0.114 V, respectively. It means that electrode surface covered by Au NPs is characterized by a worse reversibility compared to ITO or Au-disk. Such behavior probably results from the increase of ITO resistance due to thermal treatment performed at 500 °C. Indeed, the change of resistance of pure ITO upon calcination from 25 Ω at room temperature up to 150 Ω after 90 min of annealing is observed in our case, in agreement with other reports [42, 43]. Thus, on the contrary to laser annealing used for Au NP formation on ITO substrate [19, 26, 39], the thermal treatment in furnace have negative impact on ITO electric properties which in turn affects the electrochemical activity. Nevertheless, despite ΔE increases, the observed electrode reversibility is still satisfactory.

The cyclic voltammetry response of different electrodes in the presence of glucose in 0.1 M KOH is shown in Fig. 8. The description of the whole mechanism concerning glucose oxidation at Au nanoparticles is given in details in our previous work [19]. In short, the CV curve of the nanosized electrode in glucose alkaline media shows three electrochemical processes during the anodic polarization and one—when electrode is cathodically polarized. During the positive potential scan, the gradual increase in current is observed. The peaks with

maxima located at ca. 0.11 V vs. Ag/AgCl/0.1 M KCl are characterized by a wide left shoulder due to several oxidative processes: (A) electrosorption of glucose followed by formation of gluconolactone intermediate, (B) increase of AuOH sites and subsequent gluconolactone oxidation, and finally (C) generation of gold oxides on the electrode surface. On the other hand, the negative potential scan shows that a reduction in the surface gold oxides occurs and thus enough surface active states are available for the direct oxidation of glucose resulting in a sharp anodic peak (D) observed at 0.044 V vs. Ag/AgCl/0.1 M KCl. On the contrary to Au-disk and Au-NP-modified electrodes, no electrochemical processes were detected for ITO as working electrode. Comparing the current densities, one may observe that the current value at the D-peak maximum increases with the duration of thermal treatment of the ITO/Au substrates. Such behavior is always related with the change in electrochemically active surface area. Because the interparticle distance for obtained materials decreases with the dewetting time, both the highest active surface area of Au NPs and simultaneously the highest peak current are observed for ITO/Au-5 nm-80 min sample.

Furthermore, it should be noted that the oxidative peak of ITO/Au-5 nm-80 min in the negative scan is shifted anodically by 33 mV comparing to Au disk electrode, whereas the oxidative peak registered at negative polarization is shifted toward the cathodic region by 95 mV. Similar observations were

**Fig. 6** Raman spectra of rhodamine 6G deposited on structures shown in Fig. 3**Fig. 7** Cyclic voltammograms of ITO, Au-disk, and AuNPs/ITO in 10 mM $K_3Fe(CN)_6$ + 1 M KCl registered at 50 mV/s

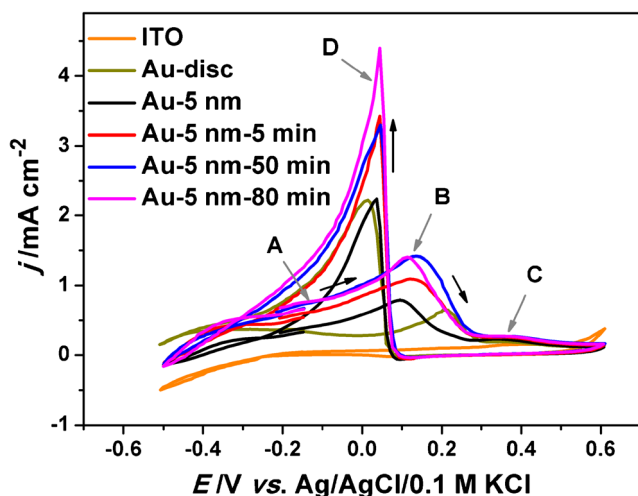


Fig. 8 Cyclic voltammograms obtained at different electrode surfaces immersed in 0.1 M KOH with 10 mM of glucose

reported by Pasta et al. but in the case of different electrolyte pH [44]. According to reported results, the increase in current with simultaneous positive shift of the D peak was observed when electrolyte pH has changed from neutral to basic. Positive shift of the D-maximum position could be attributed to decrease of the active sites upon thermal treatment but the simultaneous peak current enhancement is closely related with the increase in active surface area. This second effect is predominant thus the difference in current densities between Au-disk and Au-5 nm-80 min is significant.

Conclusions

For gold nanoarrays produced via thermal dewetting process, the morphology, optical, spectroscopic, and electrochemical properties were investigated. The samples ($10 \times 10 \text{ mm}^2$) were prepared from Au thin films deposited on ITO-coated substrates. It was found that thermal annealing ensured the homogenous distribution of NPs on the whole treated area, and the process can be easily scaled-up to industrial applications. Up to 25% coverage of ITO by NPs has been estimated, and this value is comparable with that obtained for the best samples produced by laser dewetting in our previous work. From SEM images, the disk-like and nearly spherical shape and size not exceeding 80 nm in dependence on preparation time were deduced. The regularity and interparticle distances were concluded from FFT processing of the SEM pictures. The electrode performance has been confirmed by SERS measurements showing the enhancement factor of Raman signal of 10^7 – 10^8 . The CV measurements performed in 10 mM of ferricyanide and glucose solutions showed that Au NP-modified ITO exhibits much higher electrochemical activity than Au layer or Au-disk electrode. The highest peak currents

were registered for ITO/Au thermally treated for 80 min similarly to SERS performance of this electrode material.

However, because electric properties of the ITO substrate undergo degradation due to thermal treatment, further experiments will concern application of the FTO glass for Au deposition and thermal annealing.

Acknowledgements KG and KS acknowledge the National Science Centre of Poland, NCN, for the financial support under contracts 2012/07/N/ST5/02139 and 2012/07/D/ST5/02269, respectively. The authors appreciate also the inspiration toward electrochemical sensing from the Cost Action MP 1202 HINT.

References

- Eustis S, El-Sayed MA (2006) Why gold nanoparticles are more precious than pretty gold: noble metal surface plasmon resonance and its enhancement of the radiative and nonradiative properties of nanocrystals of different shapes. *Chem Soc Rev* 35:209–217
- Kelly KL, Coronado E, Zhao LL, Schatz GC (2003) The optical properties of metal nanoparticles: the influence of size, shape and dielectric environment. *J Phys Chem B* 107:668–677
- Prasad PN (2004) *Nanophotonics*. John Wiley & Sons, Inc, Hoboken
- Plante MC, LaPierre RR (2008) Au-assisted growth of GaAs nanowires by gas source molecular beam epitaxy: tapering, sidewall faceting and crystal structure. *J Cryst Growth* 310:356–363
- Gu YL, St-Pierre J, Ploehn HJ (2008) Pt/glassy carbon model catalyst prepared from PS-b-P2VP micellar templates. *Langmuir* 24:12680–12689
- Haes AJ, Hall WP, Chang L, Klein WL, Duyne RP (2004) A localized surface plasmon resonance biosensor: first steps toward an assay for Alzheimer's disease. *Nano Lett* 4:1029–1034
- Malek K, Brzozka A, Rygula A, Sulka G (2014) SERS imaging of silver coated nanostructured Al and Al₂O₃ substrates. The effect of nanostructure. *J Raman Spectrosc* 45:281–291
- Hyeon T (2003) Chemical synthesis of magnetic nanoparticles. *Chem Commun* 927–934. doi:10.1039/B207789B
- Karim W, Tschupp SA, Oezaslan M, Schmidt TJ, Gobrecht J, van Bokhoven JA, Ekinci Y (2015) High-resolution and large-area nanoparticle arrays using EUV interference lithography. *Nanoscale* 7:7386–7393
- Marrian CRK, Tennant DM (2003) Nanofabrication. *J Vac Sci Technol A* 21:S207–S215
- Tsuda T, Sakamoto T, Nishimura Y, Seino S, Imanishi A, Kuwabata S (2012) Various metal nanoparticles produced by accelerated electron beam irradiation of room-temperature ionic liquid. *Chem Commun* 48:1925–1927
- Noriki T, Abe S, Kajikawa K, Shimoyo M (2015) Patterning technique for gold nanoparticles on substrates using a focused electron beam. *Beilstein J Nanotechnol* 6:1010–1015
- Garcia R, Knoll AW, Riedo E (2014) Advanced scanning probe lithography. *Nat Nanotechnol* 9:577–587
- Oh Y-J, Kim J-H, Thompson CV, Ross CA (2013) Templated assembly of Co-Pt nanoparticles via thermal and laser-induced dewetting of bilayer metal films. *Nanoscale* 5:401–407
- Grochowska K, Śliwiński G (2012) Quality investigation of Au nanoarrays for biosensing applications. *Solid State Phenom* 183: 81–88
- Ruffino F, Carria E, Kimiagar S, Crupi I, Simone F, Grimaldi MG (2012) Formation and evolution of nanoscale metal structures on

- ITO surface by nanosecond laser irradiations of thin Au and Ag films. *Sci Adv Mater* 4:708–718
17. Grochowska K, Nedyalkov N, Atanasov P, Śliwiński G (2011) Nanostructuring of thin Au films by means of short UV laser pulses. *Opto-Electron Rev* 19:327–332
 18. Nikov RG, Nedyalkov NN, Atanasov PA, Hirsch D, Rauschenbach B, Grochowska K, Śliwiński G (2016) Characterization of Ag nanostructures fabricated by laser-induced dewetting of thin films. *Appl Surf Sci* 374:36–41
 19. Grochowska K, Siuzdak K, Karczewski J, Śliwiński G (2015) Functionalization of indium-tin-oxide electrodes by laser-nanostructured gold thin films for biosensing applications. *Appl Surf Sci* 357:1684–1691
 20. Kerkache L, Layadi A, Dogheche E, Remiens DD (2006) Physical properties of RF sputtered ITO thin films and annealing effect. *J Phys D Appl Phys* 39:184–189
 21. Park J-O, Lee J-H, Kim J-J, Cho S-H, Cho YK (2005) Crystallization of indium tin oxide thin films prepared by RF-magnetron sputtering without external heating. *Thin Solid Films* 474:127–132
 22. Jung YS, Lee DW, Jeon DY (2004) Influence of dc magnetron sputtering parameters on surface morphology of indium tin oxide thin films. *Appl Surf Sci* 221:136–142
 23. Wang L, Mao W, Ni D, Di J, Wu Y, Tu Y (2008) Direct electrodeposition of gold nanoparticles onto indium/tin oxide film coated glass and its application for electrochemical biosensor. *Electrochem Commun* 10:673–676
 24. Zhang J, Oyama M (2004) A hydrogen peroxide sensor based on the peroxidase activity of hemoglobin immobilized on gold nanoparticles-modified ITO electrode. *Electrochim Acta* 50:85–90
 25. Wu M, Yuan D, Yu J, Chen H (2013) Sensitive electrochemiluminescence biosensor based on Au-ITO hybrid bipolar electrode amplification system for cell surface protein detection. *Anal Chem* 85:11960–11965
 26. Grochowska K, Siuzdak K, Śliwiński G (2015) Properties of indium tin oxide electrode modified by a laser nanostructured thin Au film for biosensing. *Eur J Inorg Chem* 7:1275–1281
 27. Botta R, Upender G, Bansal C (2015) Silver nanocluster films on ITO coated glass as novel substrates for the detection of molecules using surface enhanced Raman scattering (SERS). *IOP Conf Ser: Mater Sci Eng* 73:012143
 28. Shu H, Chang G, Wang Z, Li P, Zhang Y, He Y (2015) Pulse laser deposition fabricating gold nanoclusters on a glassy carbon surface for nonenzymatic glucose sensing. *Anal Sci* 31:609–616
 29. Chen H, Wang Y, Qu J, Dong S (2007) Self-assembled silver nanoparticle monolayer on glassy carbon: an approach to SERS substrate. *J Raman Spectrosc* 38:1444–1448
 30. El-Sayed HA, Horwood CA, Owusu-Ansah E, Shi YJ, Birss VI (2015) Gold nanoparticle array formation on dimpled Ta templates using pulsed laser-induced thin film dewetting. *Phys Chem Chem Phys* 17:11062–11069
 31. Krishna H, Shirato N, Favazza C, Kalyanaraman R (2011) Pulsed laser-induced self-organization by dewetting of metallic films. *J Mater Res* 26:154–169
 32. Haiss W, Thanh NTK, Aveyard J, Fernig DG (2007) Determination of size and concentration of gold nanoparticles from UV-Vis spectra. *Anal Chem* 79:4215–4221
 33. Simsek E (2009) Effective refractive index approximation and surface plasmon resonance modes of metal nanoparticle chains and arrays. *PIERS Online* 5:629–632
 34. Hoggard A, Wang L-Y, Ma L, Fang Y, You G, Olson J, Liu Z, Chang W-S, Ajayan PM, Link S (2013) Using the plasmon linewidth to calculate the time and efficiency of electron transfer between gold nanorods and grapheme. *ACS Nano* 7:11209–11217
 35. Bigot I-Y, Halte W, Merle J-C, Daunois A (2000) Electron dynamics in metallic nanoparticles. *Chem Phys* 251:181–203
 36. Imamova SE, Dikovska A, Nedyalkov NN, Atanasov PA, Sawczak M, Jendrzewski R, Śliwiński G (2010) Laser nanostructuring of thin Au films for application in surface enhanced Raman spectroscopy. *J Optoelectron Adv Mater* 12:500–504
 37. Fazio E, Neri F, D'Andrea C, Ossi PM, Santo N, Trusso S (2011) SERS activity of pulsed laser ablated silver thin films with controlled nanostructure. *J Raman Spectrosc* 42:1298–1304
 38. Gupta R, Weimer WA (2003) High enhancement factor gold films for surface enhanced Raman spectroscopy. *Chem Phys Lett* 374:302–306
 39. Grochowska K, Siuzdak K, Atanasov PA, Bittencourt C, Dikovska A, Nedyalkov NN, Śliwiński G (2014) Properties of plasmonic arrays produced by pulsed-laser nanostructuring of thin Au films. *Beilstein J Nanotechnol* 5:2102–2112
 40. Ballarin B, Cassani MC, Maccato C, Gasparotto A (2011) RF-sputtering preparation of gold-nanoparticles-modified ITO electrodes for electrocatalytic applications. *Nanotechnology* 22:275711
 41. Wang J, Cao X, Wang X, Yang S, Wang R (2014) Electrochemical oxidation and determination of glucose in alkaline media based on Au (111)-like nanoparticle array on indium tin oxide electrode. *Electrochim Acta* 138:174–186
 42. Kim YN, Shin HG, Song JK, Cho DH, Lee HS, Jung YG (2005) Thermal degradation behavior of indium tin oxide thin films deposited by radio frequency magnetron sputtering. *J Mater Res* 20:1574–1579
 43. Kalyanasudaram K (2010) Dye sensitized solar cells. EPFL Press, Lausanne
 44. Pasta M, Mantia FL, Cui Y (2010) Mechanism of glucose electrochemical oxidation on gold surface. *Electrochim Acta* 55:5561–5568